Agricultural and Forest Meteorology 166–167 (2012) 127–136

Contents lists available at SciVerse ScienceDirect

Agricultural and Forest Meteorology

journal homepage: www.elsevier.com/locate/agrformet

Predictive model for scalar concentration fluctuations in and above a model plant canopy

John V. Postma[a,*], Eugene Yee[b], John D. Wilson[a]

[a] Department of Earth and Atmospheric Sciences, University of Alberta, Edmonton, AB T6G 2E3, Canada
[b] Defence R&D Canada - Suffield, P.O. Box 4000, Medicine Hat, AB T1A 8K6, Canada

ARTICLE INFO

Article history:
Received 6 December 2011
Received in revised form 17 June 2012
Accepted 25 June 2012

Keywords:
Canopy flow
Concentration fluctuations
Micromixing model
Scalar dissipation

ABSTRACT

A Lagrangian stochastic (LS) implementation of an interaction by exchange with the conditional mean (IECM) micromixing model is used to estimate concentration fluctuations in plumes dispersing from an in-canopy, localized source into a model plant canopy flow. The sensitivity of the LS-IECM model to the underlying Eulerian flow statistics is investigated by comparing model predictions from simulations driven by two interpolations of the same water-channel flow data. The two simulations showed minor differences in the predicted mean concentration but marked differences in the standard deviation, skewness and kurtosis of concentration. This is shown to be caused by differences in the turbulent kinetic energy (TKE) dissipation rates between the two interpolations and their effects on the IECM model. The LS-IECM model predictions of the first four moments of the scalar concentration field showed fair to good conformance (depending on which TKE dissipation rate is used) with experimental water-channel dispersion data.

1. Introduction

Chemotaxis is a phenomenon through which insects can locate food and mates by modulating their travel paths in response to chemical signals (Murlis et al., 1992 and references therein). If the insect is seeking pollen then pollination may occur, benefiting the agricultural and forest sectors. However, if this insect carries a disease or is herbivorous then crop and economic losses may result. Some species, such as bark beetles, emit an aggregation pheromone to signal other beetles to a feeding location in an effort to overcome a tree's natural defenses. This pheromone and, more importantly, the corresponding anti-aggregation pheromone can be synthesized and used to prevent colonization of bark beetles into new areas (e.g., Graves et al., 2008; Gillette et al., 2009). The mixed success so far achieved by this practice is due to a lack of understanding of the biology of insect odour detection and the complexity of odour dispersion within a forest canopy (e.g., Vickers, 2000). The odour concentrations within canopy flows are often highly intermittent, with high concentrations frequently followed by near-zero concentrations at a measurement location. This is caused by the meandering, entrainment and dissipation of the odour plume. Some insects may be sensitive to these variations of concentration (Baker et al., 1998; Murlis, 1997) and therefore an improved understanding of the dispersion process in canopy flow and the resulting concentration fluctuations would be beneficial to agricultural and forest managers.

Advances in computer power and an increase in the availability of computational resources have made possible the prediction of concentration fluctuations in atmospheric dispersion models. A variety of different modelling techniques have been employed to this end: solving the Reynolds-averaged Navier–Stokes equation and scalar transport equation, along with various closure assumptions (Hsieh et al., 2007; Wang et al., 2009), fluctuating plume models (Gifford, 1959) with added parametrization for relative, in-plume concentration fluctuations (Yee et al., 1994; Luhar et al., 2000; Yee and Wilson, 2000; Franzese, 2003; Gailis et al., 2007), and probability density function (PDF) modelling techniques (Sawford, 2004a,b; Luhar and Sawford, 2005; Cassiani et al., 2005a,b,c, 2007; Yee et al., 2009; Postma et al., 2011a,b). This last approach is followed here.

The Sequential Particle MicroMixing Model (SPMMM) couples a three-dimensional Lagrangian stochastic (LS) trajectory model (see Rodean, 1996 for a review) with the Interaction by Exchange with the Conditional Mean (IECM) micromixing model (Fox, 1996; Pope, 1998). To "drive" the dispersion in LS models, a statistical description of the flow field such as the mean winds, Reynolds stresses and turbulent kinetic energy (TKE) dissipation rate must be provided. These "driving flow statistics" may come from full-scale field experiments, water-channel or wind-tunnel experiments or from another numerical model. A strength of LS trajectory models is their ability to represent many scales of motion, from extremely small

* Corresponding author. Tel.: +1 867 633 5913.
E-mail addresses: jpostma@ualberta.ca, postmajv@yahoo.ca (J.V. Postma), eugene.yee@drdc-rddc.gc.ca (E. Yee), jaydee.uu@ualberta.ca (J.D. Wilson).

0168-1923/$ – see front matter © 2012 Elsevier B.V. All rights reserved.
http://dx.doi.org/10.1016/j.agrformet.2012.06.016

to extremely large. However, the underlying Eulerian fields used to drive the LS models are often provided on a relatively coarse grid. To realise the full potential of the scale-free nature of LS models, it is advantageous to perform some form of interpolation of the relatively coarse experimental data onto a finer numerical grid. Interpolation schemes can produce profiles that pass through the experimental data or use it as a guide. Both techniques can result in a smooth profile, but conforming to the data exactly often results in a profile which contains oscillations or ringing between the measurements. It is unknown whether this ringing is consistent with reality, and certainly only additional flow measurements can address this issue.

In this study, we investigate the accuracy with which SPMMM can predict the first four moments of the scalar concentration field (mean, standard deviation, skewness and kurtosis) resulting from the release of a passive scalar from an in-canopy, localized source into a neutrally stratified model plant canopy flow. Furthermore, the sensitivity of SPMMM to the driving flow statistics is investigated by comparing results from simulations driven by two different piecewise, cubic polynomial interpolations of the experimental driving flow statistics.

2. Setup

2.1. SPMMM

A full description of the governing equations and numerical implementation of SPMMM can be found in Postma et al. (2011a). Each particle has assigned to it a velocity, a position and a scalar concentration. The Lagrangian velocity fluctuation relative to the Eulerian mean $U_i' = U_i - \langle u_i \rangle$ and the Lagrangian position X_i evolve according to

$$dU_i' = a_i(\boldsymbol{X}, \boldsymbol{U}', t)\,dt + b_{ij}(\boldsymbol{X}, \boldsymbol{U}', t)\,d\xi_j(t), \tag{1}$$

$$dX_i = \left(\langle u_i \rangle + U_i'\right)\,dt, \tag{2}$$

where dt is the timestep and $d\xi_j(t)$ represents an incremental Wiener process with a mean of zero and variance equal to dt. The conditional mean acceleration a_i is deterministic and dependent upon the Reynolds stresses and their gradients. The well-mixed condition (Thomson, 1987) and the assumption of stationary, Gaussian turbulence are used to determine a_i in SPMMM. The drift coefficient b_{ij} is determined from the Kolmogorov scaling relationship for the velocity structure function in the inertial subrange implying $b_{ij} = (C_0\varepsilon)^{1/2}\delta_{ij}$, where C_0 is the Kolmogorov constant and ε is the turbulent kinetic energy (TKE) dissipation rate. The scalar concentration ϕ evolves according to the IECM micromixing model,

$$d\phi = -\frac{1}{t_m}\left(\phi - \langle \phi | \boldsymbol{u} \rangle\right) dt, \tag{3}$$

where t_m is the scalar micromixing time scale and $\langle \phi | \boldsymbol{u} \rangle = \langle \phi | \boldsymbol{u} \rangle(x, y, z, u, v, w)$ is the mean scalar concentration conditioned on the local velocity (also called the conditional mean concentration). The parametrization of the micromixing time scale used in SPMMM is based upon inertial-subrange theory and was originally proposed by Cassiani et al. (2005a).

For short and medium time scales, it is assumed that

$$t_m = \mu\left(\frac{\sigma_r^2}{\sigma_{\boldsymbol{U}_r}^2}\right)^{1/2}, \tag{4}$$

where μ is the empirically determined micromixing constant which depends upon the type of turbulence, the source configuration and the stage of development of the plume. It is treated as a free parameter. The instantaneous plume width σ_r is modelled as

$$\sigma_r^2 = \frac{d_r^2}{1 + (d_r^2 - \sigma_0^2)/(\sigma_0^2 + 2\sigma^2 T_L t)}, \tag{5}$$

where Richardson's law

$$d_r^2 = C_r \varepsilon (t + t_0)^3, \tag{6}$$

is used to calculate the root-mean-square separation between particle pairs and $T_L \equiv 2\sigma^2/(C_0\varepsilon)$ is the Lagrangian integral time scale. The constants in Eqs. (5) and (6) include: the initial source width σ_0, the Richardson constant C_r and $t_0 = t_s/C_r^{1/3}$, where $t_s = (\sigma_0^2/\varepsilon)^{1/3}$ is the characteristic time scale of the source. The variance of the Lagrangian relative velocity fluctuation $\sigma_{\boldsymbol{U}_r}^2$ is modelled (Franzese, 2003; Cassiani et al., 2005a) as

$$\sigma_{\boldsymbol{U}_r}^2 = \sigma^2\left(\frac{\sigma_r}{L}\right)^{2/3}, \tag{7}$$

with $\sigma^2 = 2k/3$ where k is the TKE and

$$L = \frac{(3\sigma^2/2)^{3/2}}{\varepsilon}, \tag{8}$$

is a characteristic length scale of the most energetic eddies. Wherever $\sigma_r > L$, the constraint $\sigma_{\boldsymbol{U}_r}^2 = \sigma^2$ is imposed. If t_m is larger than the turbulence timescale $\tau = k/\varepsilon$, then t_m is reset to τ. The turbulence timescale also applies for regions outside of the plume.

The required conditional mean concentration field is precalculated by releasing N_ϕ particles, one at a time, from the source and accumulating the amount of time they spend in each bin of the discretized position-velocity space. A dynamical grid that grows with the plume captures the details of plume growth close to the source. Once all particles have been transported outside the spatial domain, the conditional mean concentration is calculated as

$$\langle \phi | \boldsymbol{u} \rangle = \langle \phi | \boldsymbol{u} \rangle(x_I, y_J, z_K, u_L, v_M, w_N) = \frac{Q t_r^v}{\mathcal{V} N_\phi^v}, \tag{9}$$

where Q is the source strength, $t_r^v = t_r^v(x_I, y_J, z_K, u_L, v_M, w_N)$ is the total accumulated residence time, $\mathcal{V} = \mathcal{V}(x_I, y_J, z_K)$ is the volume of the spatial bin and

$$N_\phi^v = N_\phi^v(x_I, y_J, z_K, u_L, v_M, w_N) = N_\phi f_{\boldsymbol{u}} \Delta u \Delta v \Delta w, \tag{10}$$

is the number of particles during the simulation that visit bin $(x_I, y_J, z_K, u_L, v_M, w_N)$. In the above equation, $f_{\boldsymbol{u}}$ is the PDF of the velocity statistics used to drive the dispersion model and Δu, Δv and Δw are respectively the bin widths of the discretized streamwise, spanwise and vertical velocity dimensions.

In SPMMM, particles are released sequentially from the upstream face of the spatial domain and allowed to propagate downstream, mixing with the conditional mean concentration field according to Eq. (3). If a particle originates in the source area, it is assigned a non-zero initial concentration, the exact value of which depends on the source configuration and the source strength. Depending on the chosen source configuration, there are three or four free parameters that need to be set in SPMMM: the Kolmogorov constant C_0, the Richardson constant C_r and the micromixing constant μ (used in the parametrization of t_m) are the three mandatory free parameters. In addition, for an initial Gaussian source distribution, the effective source "width" σ_0 is also a free parameter, whereas for an initial top-hat distribution, this parameter is fixed by the actual source size (assumed to be known *a priori*).

SPMMM has been used to estimate with good accuracy the mean concentration and the standard deviation of concentration for plumes dispersing from elevated and ground-level compact sources in wall shear-layer flow (Postma et al., 2011a). It has also been used to estimate with fair accuracy the mean concentration

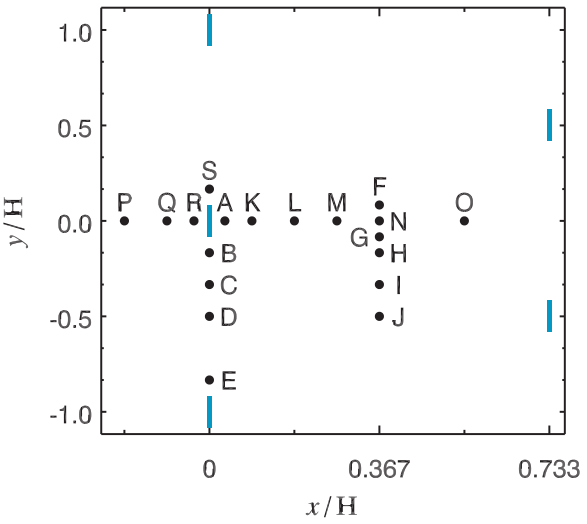

Fig. 1. A plan view of a portion of the model plant canopy. Points A–S are velocity statistic data extraction locations used by Hilderman and Chong (2007). Extraction locations A–J correspond to the extraction locations used by Raupach et al. (1986). The thin rectangles represent the canopy obstacles. Note that the axes do not use the same scale.

and the standard deviation of concentration for plumes dispersing from an elevated line source into a canopy flow (Postma et al., 2011b). This was somewhat surprising since t_m is defined in terms of inertial-subrange theory and canopy flows lack a well-defined inertial subrange. Nevertheless, it has been shown by Cassiani et al. (2007) and Postma et al. (2011b) that predictions of the first two moments of the scalar concentration field in a canopy flow using this parametrization of t_m are qualitatively and quantitatively satisfactory. It is important to note that SPMMM does not resolve the canopy obstacles. Instead, the effects of the canopy are manifested through its effects on the driving velocity statistics and the TKE dissipation rate.

In theory, SPMMM can predict any order moment of the scalar concentration field but in practice this is limited by the availability of computational resources—predictions of the higher-order moments require more particles. However, the non-interactive nature of the particles in SPMMM allows for trivial parallelization as well as simple programming and short execution times.

2.2. Model plant canopy

The model plant canopy consisted of a regular diamond-shaped array of rectangular aluminum obstacles measuring 10 mm in width, 1 mm in streamwise thickness and $H = 60$ mm in height (Raupach et al., 1986). The streamwise and spanwise centre-to-centre obstacle spacings were 44 mm and 60 mm, respectively. Wind-tunnel dispersion experiments were carried out within the canopy for an elevated plane source (Coppin et al., 1986) and an elevated line source (Legg et al., 1986). Hilderman and Chong (2007) revisited scalar dispersion in an identical canopy using a near ground-level localized source, a configuration that was not examined by the original wind-tunnel study. The latter experiments were performed in the Coanda Research and Development Corporation (Burnaby, British Columbia) recirculating water channel, with a test section measuring 10.0 m × 1.5 m × 1.0 m in length, width and depth, respectively. There were 210 rows of canopy elements within the test section of the water channel. These experiments are hereafter referred to as the *Coanda* experiments. A portion of the canopy in plan view can be seen in Fig. 1.

The water-channel flow was seeded with titanium dioxide particles to allow the extraction of velocity statistics with laser Doppler velocimetry. Measurements of the u, v, and w velocity components at 19 points (A–S) were made in the unit cell centred on the seventh tab of row 160, $x = 7.04$ m into the canopy and $y = 0.42$ m from the sidewall of the water channel. At all points, velocity measurements were made up to a height of $3H = 180$ mm. For points D and J, velocity measurements were made up to a height of $12H = 720$ mm.

The scalar source was a horizontally oriented tube with a diameter of $d_s = H/4 = 15$ mm positioned immediately behind a canopy obstacle at a height of $z_s = 0.2H = 12$ mm. Since the sharp-sided aluminum tabs are very efficient turbulence generators, Hilderman and Chong (2007) found that the concentration field resulting from dispersion from a very small source was extremely sensitive to the exact placement within the canopy, and that the plume could easily be biased to one side of the channel or the other by a slight change in the release angle or velocity. As this is undesirable from the standpoint of being able to reproduce experimental results, a relatively large source was used. The source was designed to have minimal momentum and had a fine mesh over the end, to ensure a uniform distribution of the dye over the source area. Sodium fluorescein dye was used as the dynamically passive tracer. The velocity of the dye at the source was $u_s = 2.26 \times 10^{-3}$ m s^{-1}, which corresponds to a release rate of $Q = 24$ mL min^{-1}. Sodium fluorescein is a weakly diffusive scalar, with a (molecular) Schmidt number of 1920 in water. Laser-induced fluorescence was used to extract concentration data 1, 2, 4, 7, 8, 12, and 16 rows downstream from the source at 7 to 10 heights, depending on the location. The measurements were made dimensionless by dividing by the source concentration (i.e., $\phi^* = \phi/\phi_s$). The source concentration is $\phi_s = Q/(A_s u_s)$ where A_s is the area of the source. Once dimensionless, higher-order statistical quantities were calculated. The dimensionless quantities are denoted with a superscript asterisk: $\langle\phi^*\rangle$ for the mean, σ^*_ϕ for the standard deviation, Sk^*_ϕ for the skewness and Ku^*_ϕ for the kurtosis of the dimensionless concentration.

2.3. Interpolation techniques

Two interpolation techniques are used in this study: cubic spline interpolation and Savitzky–Golay filtering (Savitzky and Golay, 1964; Steinier et al., 1972). Both techniques involve fitting piecewise polynomials to the experimental data but differ considerably in the details of the fitting. Cubic splines use third-degree polynomials to interpolate between data points. The resulting profile passes through the experimental data exactly and is continuous and smooth, as is its first derivative. Its second derivative is also continuous. Passing through the experimental data exactly is perhaps the most desirable feature of cubic spline interpolation but can result in oscillations between the data points as the curvature of the spline may have to change frequently and drastically to reach the next data point. There are a variety of end point conditions that can be imposed upon the cubic spline. The natural spline allows the spline to equilibrate such that the oscillatory nature is minimized, which is suitable for fitting a curve to experimental data.

The Savitzky–Golay filter is also known as the digital smoothing polynomial filter or the least-squares smoothing filter. It performs a least-squares polynomial fit to data within the filter window. The degree of the polynomial and the width of the filter window are variables. The Savitzky–Golay filter has as a strength the ability to maintain data features while reducing noise, provided the degree and window width are chosen carefully. In this study, we used a third-degree polynomial and a filter window width of $2H/3$ as we found that these values smoothed the experimental data while maintaining the general trends in the measurements. As originally described, the Savitzky–Golay filter required uniformly spaced data but modern algorithms have relaxed this requirement.

2.4. Driving velocity statistics

To drive the SPMMM simulations, a horizontally homogeneous flow field was produced by spatially averaging the data from points A–J. The data from points L–S filled in details between points A–J (measurement locations in the original study) and therefore were not included in the averaging. Above $3H$, the averaged velocity statistics from points D and J were used. The spatially averaged velocity statistics are shown by the symbols in Fig. 2.

From these data, the friction velocity at the top of the canopy was determined to be $u_* = 0.02\,\mathrm{m\,s^{-1}}$ and the roughness length was $z_0 = 9\,\mathrm{mm}$. The boundary layer depth was $\delta = 540\,\mathrm{mm}$ and the free-stream velocity was $\langle u\rangle_\delta = 0.175\,\mathrm{m\,s^{-1}}$, giving a Reynolds number (based on δ and $\langle u\rangle_\delta$) of $Re_\delta = 9.4\times10^4$. At the top of the canopy the mean streamwise velocity was $\langle u\rangle_c = 0.07\,\mathrm{m\,s^{-1}}$, giving $Re_c = 4.2\times10^3$ (based on H and $\langle u\rangle_c$). The lines in Fig. 2 represent the two interpolations used to drive the SPMMM simulations. The solid lines represent the cubic spline interpolations, which more closely match the experimental data resulting in "bumps" and "wiggles" in the vertical profiles. The smoother, dotted lines represent Savitzky–Golay interpolations of the experimental data. The effects of the canopy are apparent in this figure—rapid attenuation of all velocity statistics below the canopy and maxima of the stresses near the canopy top. The most notable difference between the two interpolations is that the maxima of the Savitzky–Golay interpolated stresses σ_v^2, σ_w^2 and $\langle u'w'\rangle$ are smaller than the maxima of the corresponding cubic spline interpolated stresses.

As no measurements or estimations of ε were made in the Coanda experiments, it was approximated as the sum of wake and shear production of TKE: $\varepsilon \approx P_s + P_w$. Both the shear production of TKE, $P_s = -\langle u'w'\rangle\,\partial\langle u\rangle/\partial z$ and the wake production of TKE, $P_w = -\langle u\rangle\,\partial\langle u'w'\rangle/\partial z$ are in closed form and readily calculated from the measured velocity statistics. This approximation ignores the turbulent transport of TKE since it has no closed form and therefore would have had to be modelled, introducing other tunable parameters into the model. We viewed this as undesirable. Since turbulent transport was a major loss in the TKE budget just above the canopy and was the principal gain within the upper canopy in the wind-tunnel experiments (Raupach et al., 1986), the above approximation is subject to error. However, in Postma et al. (2011b) the approximation was shown to produce a vertical profile of the TKE dissipation rate that conformed well with data from the wind-tunnel experiments. The resulting profiles shown in Fig. 2 seem reasonable, having their maxima near the canopy top and rapidly attenuating above and below it. The Savitzky–Golay interpolated TKE dissipation rate has its larger maximum slightly higher in the canopy and experiences greater attenuation below the canopy than the cubic spline interpolated TKE dissipation rate.

This experimental data set could be used to investigate whether the use of inhomogeneous velocity statistics (e.g, the statistics from points A-S) results in more accurate model predictions than the use of horizontally homogeneous velocity statistics (e.g., the spatially averaged statistics described above). However, the use of strongly inhomogeneous velocity statistics may result in the generation of unrealistically high particle velocities which can strongly affect model predictions, particularly for the higher-order concentration moments (Postma et al., 2012) and therefore this is left for a future study.

2.5. Free parameters and discretization

The experimental source configuration is well represented by a top-hat initial source distribution. Therefore, σ_0 is set equal to the source diameter and the initial concentrations of those particles originating in the source region are given by ϕ_s (see end of Section 2.2). The remaining free parameters were set to $C_0 = 2.0$, $C_r = 0.12$ and $\mu = 0.75$. These values of C_0 and C_r are identical to those used by Postma et al. (2011a). The value of μ has been decreased from 0.82 (suitable for a line source) to 0.75 (suitable for a localized source) due to the difference in the source configuration. This reduction of the micromixing timescale reflects the increased dimensionality of the localized source configuration—entrainment of the scalar occurs in both the lateral and vertical directions whereas it occurs only in the vertical direction for a line source, and thus the micromixing constant should be reduced (Thomson, 1996; Sawford, 2004b). The value $\mu = 0.75$ was used by Postma et al. (2011a) for simulations of dispersion from a localized source.

The required conditional mean concentration field was pre-calculated in a domain that was divided into 60 bins in the x, y, and z directions and 20 bins in the u, v, and w dimensions. The timestep was chosen to be two percent of either the Lagrangian integral timescale or the mixing timescale, whichever was smaller. The pre-calculation of the conditional mean concentrations utilized 5×10^7 particles while the micromixing phase of the simulations utilized 10^8 particles. More particles were needed in the micromixing phase of the simulation in order to reduce the statistical noise in the predictions of skewness and kurtosis of concentration. Even with 10^8 particles, SPMMM simulations were quite fast, taking approximately two hours to run on a quad-core desktop computer.

3. Results and discussion

Results for two SPMMM simulations are presented below. The SPMMM-CS simulations utilized the cubic spline interpolated flow statistics to drive the model while the SPMMM-SG simulations used the Savitzky–Golay interpolated flow statistics. The SPMMM predictions[1] for the first four moments of the scalar concentration field were compared with experimental data at 12 xz-positions. At the $x/H = 1.40$, 2.87, 5.80 and 11.67 downstream locations (corresponding to 2, 4, 8 and 16 rows downstream from the source), the comparison heights $z/H = 0.1$ and $z/H = 1.0$ were used. The third comparison height farther above the canopy varied with the downstream location: $z/H = 1.5$, 2.0, 2.0 and 3.0 for the respective x/H positions. At each of the xz-positions, the measured data and the SPMMM predictions were compared across the full extent of the spanwise domain, for a total of $n = 482$ comparison pairs.

3.1. Concentration moments

The SPMMM predictions were evaluated with three performance measures. The fractional bias,

$$\mathrm{FB} = \frac{(\overline{Q_o} - \overline{Q_p})}{0.5(\overline{Q_o} + \overline{Q_p})}, \tag{11}$$

quantifies the systematic bias of the model (i.e., the difference between the observed and predicted quantities $Q_o - Q_p$). An observed quantity (water-channel data) is denoted by Q_o and a predicted quantity (SPMMM prediction) is denoted by Q_p. An overbar indicates an arithmetic mean of the available observations or predictions. A positive (negative) FB corresponds to model underprediction (overprediction). The normalised mean square error,

$$\mathrm{NMSE} = \frac{\overline{(Q_o - Q_p)^2}}{\overline{Q_o}\;\overline{Q_p}}, \tag{12}$$

[1] If a result or comment is applicable to both the SPMMM-CS and SPMMM-SG predictions or simulations then they will be collectively referred to as the SPMMM predictions or simulations

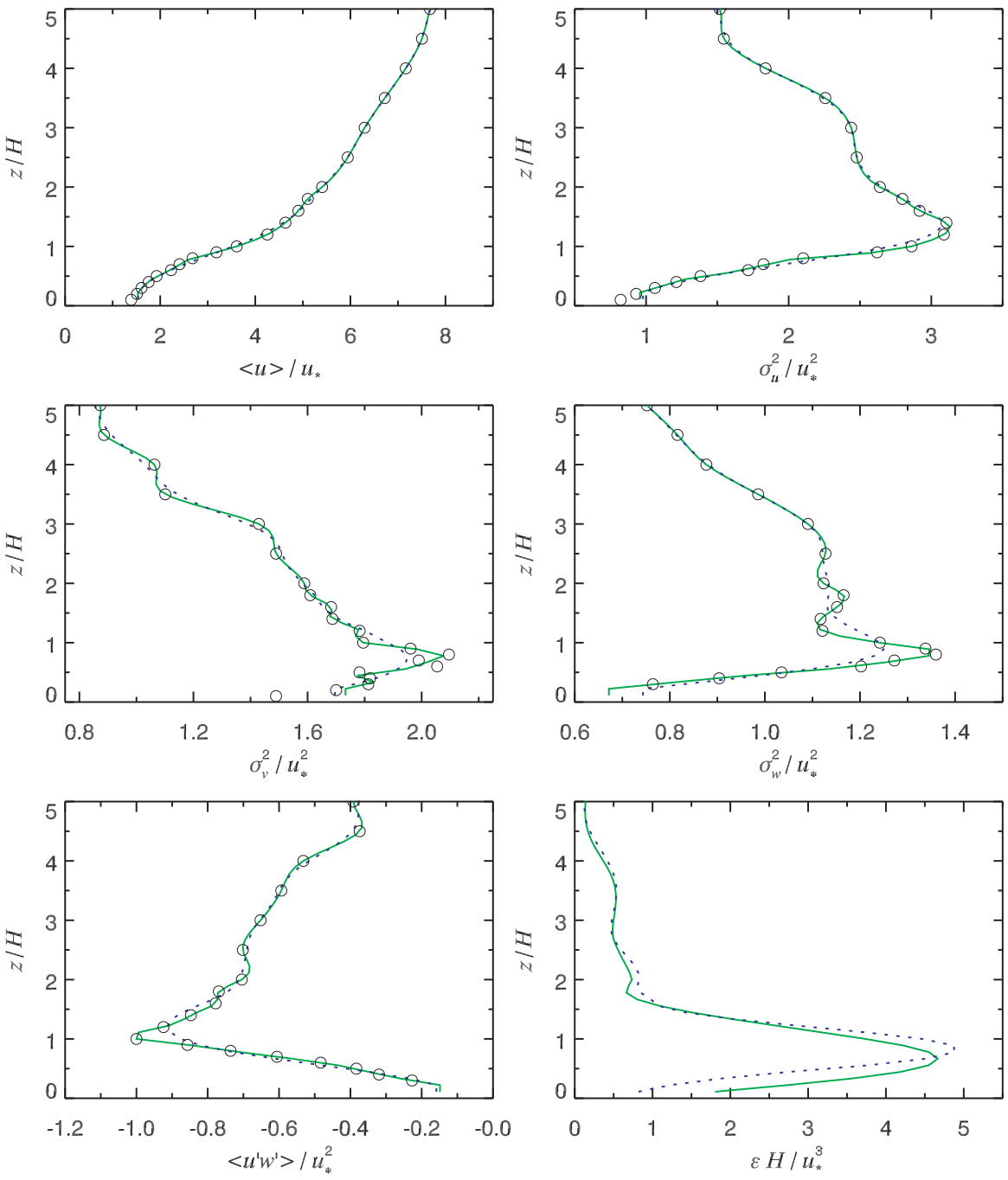

Fig. 2. Vertical profiles of the spatially averaged velocity statistics and TKE dissipation rate from the Coanda water-channel experiments. The *circles* represent the experimental data, the *solid lines* are cubic spline interpolations and the *dotted lines* are Savitzky–Golay interpolations of the data. No measurements of the TKE dissipation were taken.

quantifies the mean relative scatter of the model predictions. The FAC2 is defined as,

$$\text{FAC2} = \text{fraction of data that satisfy } 0.5 \le \frac{Q_p}{Q_o} \le 2.0. \tag{13}$$

A perfect model would have: FB = 0, NMSE = 0 and FAC2 = 1. Chang and Hanna (2004) suggest that an acceptable model should have: $-0.3 < \text{FB} < 0.3$, $\text{NMSE} < 4$ and $\text{FAC2} > 0.5$. It is possible for a non-perfect model to have FB = 0 if underprediction exactly cancels overprediction. The performance measures for the SPMMM-CS and SPMMM-SG simulations are shown in Table 1.

Streamwise transects of the concentration moments for the plume centre line ($y/H = 0$) at three heights are shown in Fig. 3.

Table 1
Performance measures for the SPMMM-CS and SPMMM-SG simulations calculated over the spanwise domain of the 12 *xz*-positions ($n = 482$).

Statistic	Simulation	FB	NMSE	FAC2
$\langle\phi^*\rangle$	CS	−0.46	1.06	0.66
	SG	−0.52	0.83	0.33
σ^*_ϕ	CS	−0.08	0.13	0.96
	SG	−0.48	0.77	0.63
Sk^*_ϕ	CS	0.28	0.50	0.78
	SG	−0.22	0.44	0.58
Ku^*_ϕ	CS	0.70	8.20	0.45
	SG	−0.02	5.17	0.36

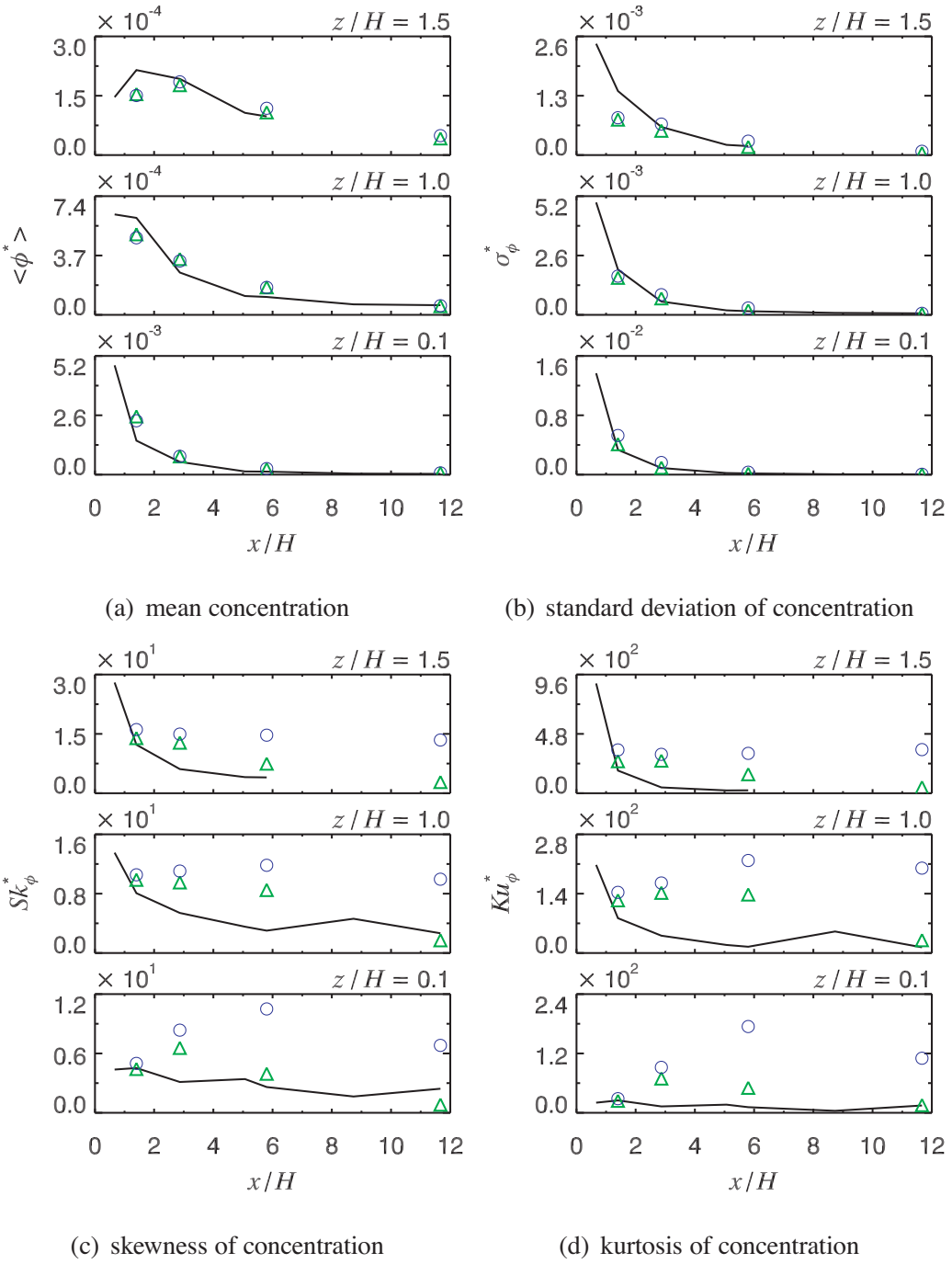

Fig. 3. Streamwise transects of the first four concentration moments for the plume centre line ($y/H = 0$). The *solid line* shows the Coanda data, the *triangles* show the SPMMM-CS predictions and the *circles* show the SPMMM-SG predictions. The vertical positions are shown on the panels. The Coanda measurements did not cover all heights at all downstream positions and therefore the lines do not extend across the full streamwise domain in the $z/H = 1.5$ panels: (a) mean concentration, (b) standard deviation of concentration, (c) skewness of concentration and (d) kurtosis of concentration.

Spanwise transects of the concentrations moments at three heights for $x/H = 11.67$ are shown in Figs. 4 and 5.

These results display the better performance of the SPMMM-CS simulations. Qualitatively, the SPMMM-CS and SPMMM-SG predictions of the mean concentration are very similar at all comparison locations. Minor differences in the transects are attributable to the minor differences in the driving velocity statistics and TKE dissipation rates. Excluding any stochastic effects, particles originating at exactly the same location in the two SPMMM simulations will follow slightly different trajectories due to differences in the underlying Eulerian fields used to drive the two simulations.

The predictions of mean concentration shown in Figs. 3(a) and 4 show a combination of under and overprediction depending on the downstream position and the height. Both simulations tended to overpredict the mean concentration within the canopy ($z/H < 1$; resulting in a negative FB that is outside of its acceptable range) which may be a result of particles being trapped below the canopy. This below-canopy overprediction was also observed in predictions of mean concentration for dispersion from an above-canopy line source using SPMMM (Postma et al., 2011b) and a similar model (Cassiani et al., 2007). The below-canopy overprediction is balanced by above-canopy underprediction, which is most

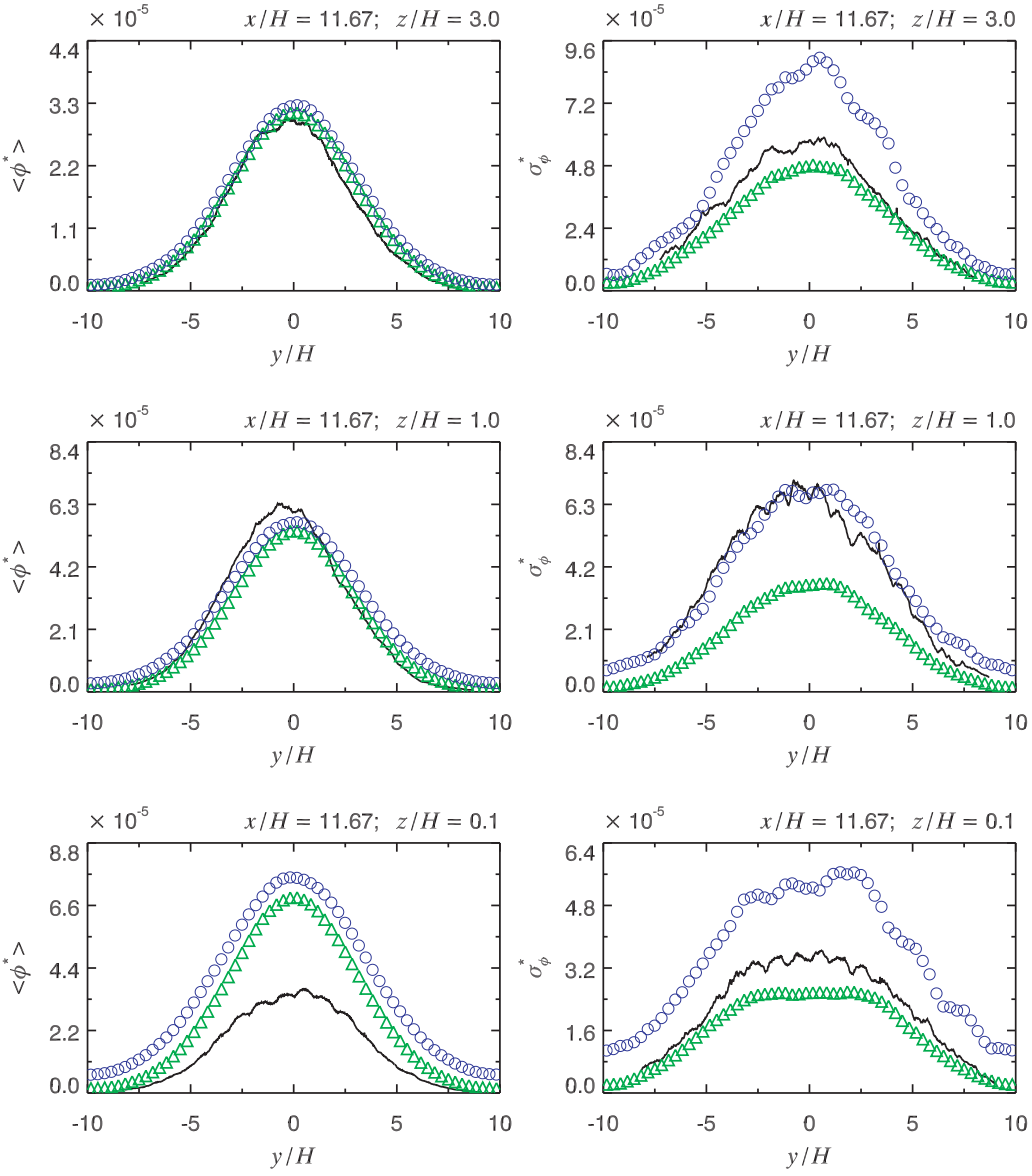

Fig. 4. Spanwise transects of mean concentration (*left column*) and standard deviation of concentration (*right column*). The *solid line* shows the Coanda data, the *triangles* show the SPMMM-CS predictions and the *circles* show the SPMMM-SG predictions. The downstream and vertical positions are shown on the panels.

pronounced near the top edge of the plume at positions closer to the source. The $x/H = 1.40$ location in Fig. 3(a) demonstrates this as does the $x/H = 2.87$ location to a lesser extent. This occurs at the $x/H = 5.80$ and 11.67 positions too but is not shown in the figures as the upper edge of the plume has grown to be above the heights shown in Figs. 3(a) and 4. Predictions above the canopy but away from the plume edge were generally quite good as is demonstrated in the $z/H = 1$ panels of Figs. 3(a) and 4. As shown in Fig. 3(a), the accuracy of the SPMMM predictions of $\langle \phi^* \rangle$ remained more or less the same with increasing downstream distance.

These results suggest that even though SPMMM performed acceptably (particularly the SPMMM-CS simulations), the vertical distribution of material in the SPMMM simulated plume is not as accurate as it could be. This may be due to simplifications to the driving velocity statistics (e.g., assumption of horizontal homogeneity) or to the fact that SPMMM does not resolve canopy obstacles. When a fluid encounters an obstacle, it may be deflected over and around the obstacle. This process could be represented by an inhomogenous flow field. For example, several of the data extraction locations behind the tabs in Fig. 1 (e.g., A, K, L, M, N, F, G, O) display mean vertical velocities greater than zero for $z/H \leq 1$. In addition, directly in front of the tab (e.g., points Q and R) the mean vertical velocities are greater than zero at the canopy top ($z/H = 1$), presumably the result of the water being deflected over the tab. These positive vertical velocities would help eject material out of the canopy and potentially reduce the below-canopy overpredictions and the upper-edge underpredictions. In contrast, the spatially averaged mean vertical velocity was approximately zero, which does not aid in the removal of material from the canopy. This process of deflection over and around the obstacles could in part be represented numerically (regardless of the flow: horizontally homogeneous or inhomogenous) by explicitly resolving the canopy obstacles and treating them as reflection surfaces. An important consequence of this treatment is that marked fluid particles would be reflected from the various resolved surfaces of the obstacles, and provide a physical mechanism that would allow these particles to more readily escape the canopy.

The assumption of Gaussian turbulence likely did not negatively affect the SPMMM predictions of mean concentration, as Flesch and Wilson (1992) demonstrated that the use of non-Gaussian velocity

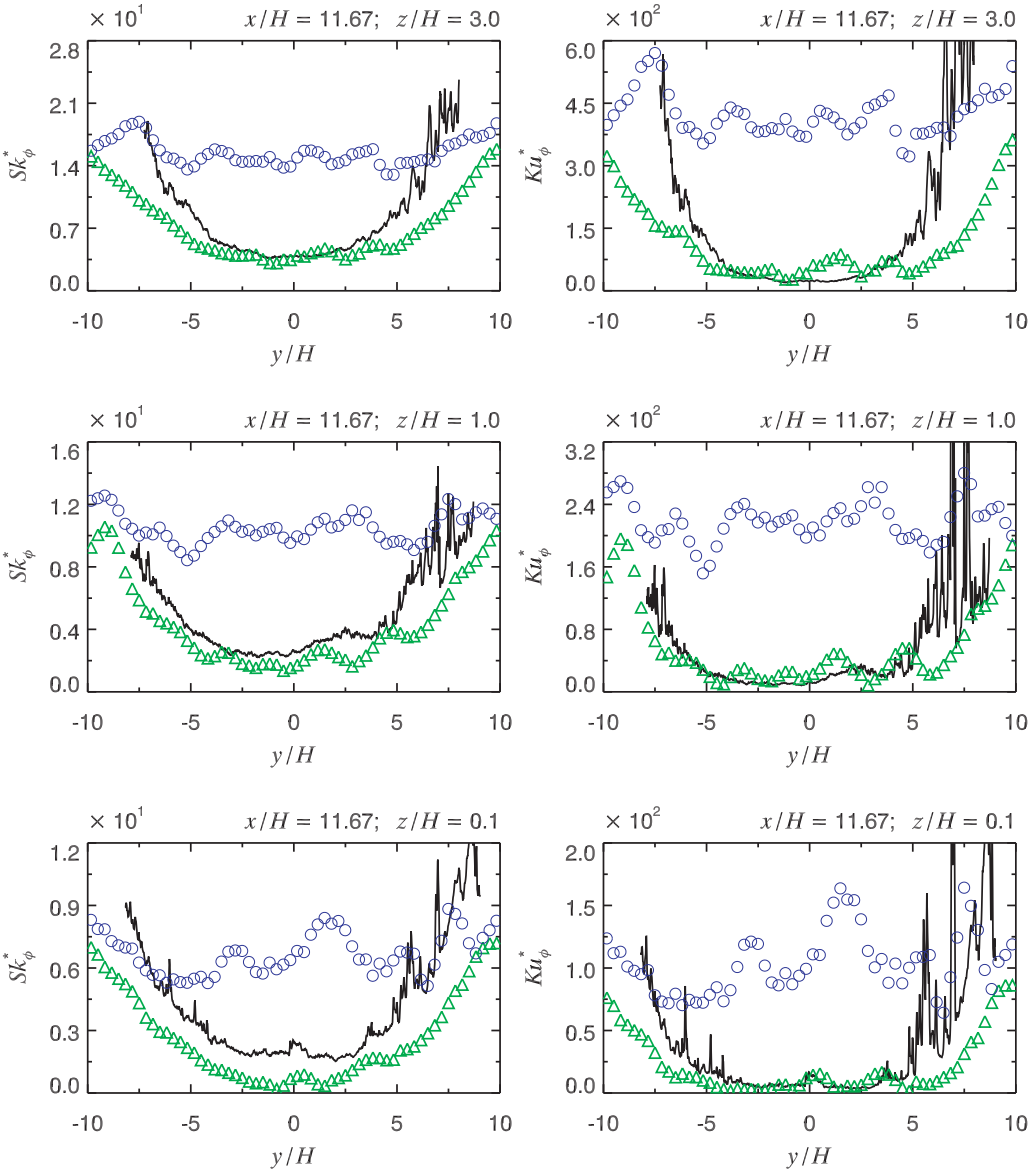

Fig. 5. Spanwise transects of skewness (*left column*) and kurtosis (*right column*) of concentration. The *solid line* shows the Coanda data, the *triangles* show the SPMMM-CS predictions and the *circles* show the SPMMM-SG predictions. The downstream and vertical positions are shown on the panels.

statistics does not improve LS model performance (at least as far as the mean concentration is concerned). The FAC2 for the SPMMM-SG simulation is half that of the FAC2 for the SPMMM-CS simulation due to an overprediction at the lateral plume edges caused by a less accurate spanwise spread of the mean concentration transects. This can be seen in Fig. 4. Since the mean concentration is very small along the plume edges, it is easier for overprediction to occur.

The three performance measures are well within their acceptable ranges for the SPMMM predictions of the standard deviation of concentration. The SPMMM-CS predictions are more accurate however. The SPMMM-SG simulations predicted greater σ_ϕ^* than the SPMMM-CS simulations at all twelve comparison locations. At two of the twelve *xz*-locations: $(x/H, z/H) = (2.87, 2.0)$ and (11.67, 1.0), this resulted in better conformance between the SPMMM-SG predictions and the experimental data. At the other 10 *xz*-locations, the SPMMM-CS predictions were more accurate with respect to the maximum standard deviation of concentration and the spanwise spread. This is reflected in the performance measures. Differences in the SPMMM-CS and SPMMM-SG predictions were less pronounced closer to the source. The predictions at $x/H = 1.40$ were approximately the same but by $x/H = 11.67$ they were markedly different. This is a result of the increased travel time to reach the farther downstream positions, which amplifies the effects of differences in the micromixing timescales between the two simulations. Fig. 3(b) shows that the accuracy of the SPMMM predictions of σ_ϕ^* is good at almost all downstream locations.

The SPMMM-CS predictions of skewness of concentration are more accurate in both magnitude and general shape than the SPMMM-SG predictions. This is true at all comparison positions but is most apparent at $x/H = 11.67$. The two SPMMM simulations make very similar predictions at $x/H = 1.40$ but exhibit progressively larger differences with increasing downstream distance, as is shown in Fig. 3(c). Note that the predictions in this figure look poorer than the overall spanwise transects shown in Fig. 5 since both the Coanda skewness data and the SPMMM predictions are relatively noisy and the comparison between data and predictions is for only one point, namely at $y/H = 0$. Both SPMMM simulations

made their most accurate predictions at the $x/H = 1.40$ (excluding the plume edges where edge effects[2] affected the experimental measurements and the SPMMM predictions) and $x/H = 11.67$ comparison locations. At the $x/H = 2.87$ and 5.80 positions the skewness of concentration was generally overpredicted. However, the performance measures are within their acceptable ranges for both simulations. Note that the performance measures are negatively affected by edge effects, particularly at the $x/H = 1.40$ position, where not enough particles were released to enable the higher-order concentration moments to be computed with good accuracy. To reliably predict skewness and kurtosis of concentration on the edge of the plume, a *very* large number of particles (e.g., $N \gtrsim 10^8$) would have to be released.

The observations for the skewness of concentration apply equally well for the kurtosis of concentration. Being the next higher-order moment above skewness, more particles are needed to reliably predict it and edge effects more strongly affected the performance measures, all of which are outside of their acceptable ranges. Qualitatively, the SPMMM-CS predictions are satisfactory, particularly at the $x/H = 1.40$ and 11.67 positions. They also outperformed the SPMMM-SG predictions. At the $x/H = 2.87$ and 5.80 positions, both SPMMM simulations tended to overpredict the kurtosis of concentration. As an alternative to predicting the higher-order concentration moments such as the skewness and kurtosis, it has been demonstrated (Yee, 2009) using a large number of high-resolution concentration data sets that the one-point concentration PDF can be determined by a specification of two parameters. Models that predict only mean concentration and standard deviation of concentration well can potentially be used with an assumed concentration PDF to predict all the higher-order moments of concentration. Given this, SPMMM may be more usefully applied (depending on the complexity of the flow field and the availability of computational resources) to predict only the first two concentration moments and an assumed concentration PDF (such as a clipped gamma distribution) can be used more effectively to predict all the higher-order moments (without the disadvantage of edge effects arising from using a finite number of particles).

3.2. Sensitivity to the underlying Eulerian fields

The SPMMM predictions for mean concentration showed little sensitivity to the underlying Eulerian fields but predicted higher-order concentrations moments were strongly sensitive to the choice of the interpolating scheme. The lack of sensitivity in the first-order concentration predictions at first seems to be in conflict with the findings of Poggi et al. (2006), which showed that predictions of the mean concentration obtained from a three-dimensional LS model are strongly sensitive to the TKE dissipation rate. However, the profiles of ε used by Poggi et al. (2006) were significantly more different than the ones shown in Fig. 2, so there is no conflict between these findings. The sensitivity of the higher-order concentration moments is due to the IECM micromixing model, which in no way affects first-order concentration statistics. In particular, it is related to the parametrization of the micromixing timescale, which in turn depends upon both the driving velocity statistics and the TKE dissipation rate. To isolate the effects of the velocity statistics and the TKE dissipation rate on the SPMMM predictions, a third simulation which used the velocity statistics from the SPMMM-SG simulation and the TKE dissipation rate from the SPMMM-CS simulation was performed. This simulation, referred to as SPMMM-ε, predicted mean concentrations that were nearly identical to the SPMMM-CS and SPMMM-SG simulations. The predictions of the higher-order concentration moments were virtually indistinguishable from the the SPMMM-CS. This can be explained by the micromixing timescale as follows.

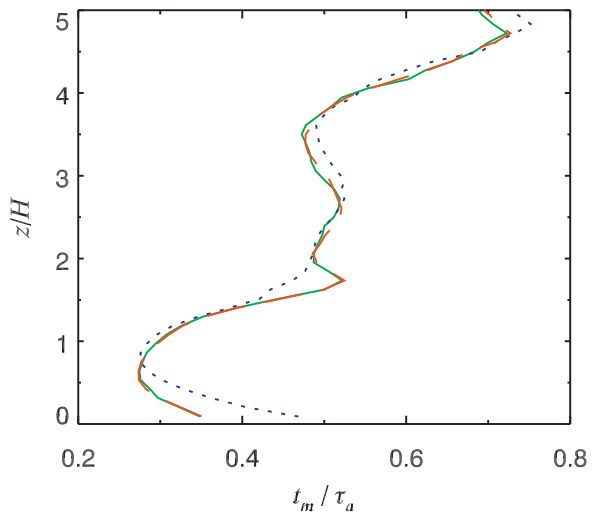

Fig. 6. Vertical profiles of the micromixing timescale for $x/H = 5.80$ (8 rows downstream from source). The mixing timescale is scaled by an advection timescale, $\tau_a = x/\langle u(z_s)\rangle$. The *solid line* is from the SPMMM-CS simulation, the *dotted line* is from the SPMMM-SG simulation and the *dashed line* is for the SPMMM-ε simulation. Note that the solid and dashed lines almost completely overlap.

Fig. 6 shows vertical profiles of the micromixing timescale for the three SPMMM simulations at $x/H = 5.80$. Other downstream locations share the same characteristics of these profiles due to the assumption of horizontal homogeneity.

The profiles from the SPMMM-CS and SPMMM-ε simulations display only minor differences between them, showing that the parametrization of the micromixing timescale used by SPMMM is more sensitive to the TKE dissipation rate than it is to the velocity statistics. At most heights, the micromixing timescale from the SPMMM-SG simulation is greater than or approximately equal to the micromixing timescale from the other two simulations. Longer micromixing timescales correspond to slower dissipation of fluctuations and therefore the SPMMM-SG simulation predicted larger standard deviation, skewness and kurtosis of concentration than the SPMMM-CS simulation.

4. Conclusions

It has been shown that the LS-IECM model SPMMM is capable of predicting with acceptable to good accuracy the first four moments of the scalar concentration field for plumes dispersing in a model plant canopy flow. The SPMMM simulations consistently overpredicted the below canopy mean concentration (resulting in a FB outside of its acceptable range) as a result of particles getting trapped within the canopy. The below-canopy overprediction is balanced by an above-canopy underprediction which is particularly marked along the upper edge of the plume. The vertical distribution of material in the plume may be better predicted by more realistic driving velocity statistics which account for the horizontally inhomogeneous and intermittent nature of canopy flow. In addition, explicit resolution of the canopy obstacles would introduce new reflection surfaces for the particles to reflect off, thereby providing another possible mechanism of escape.

Cubic spline interpolation of the underlying Eulerian velocity statistics and TKE dissipation rate was shown to produce more accurate predictions than Savitzky–Golay interpolation for the concentration moments examined. Further investigation revealed that

[2] Edge effects are an increase in noise along the plume edges due to insufficient sampling.

this was almost exclusively due to differences in the TKE dissipation rate resulting from the two interpolations. SPMMM showed a very slight sensitivity to the underlying Eulerian velocity statistics for the mean concentration and a strong sensitivity to the TKE dissipation rate for the higher-order concentration moments. This latter sensitivity was the result of the ε-dependency of the micromixing timescale. While this study demonstrated this sensitivity for one parametrization of the micromixing timescale, it likely would also affect other parametrizations that incorporate the TKE dissipation rate. The differences in the cubic spline and Savitzky–Golay interpolated TKE dissipation rate were relatively minor and yet these seemingly small differences can have marked effects, as shown. This highlights the need for careful measurement or estimation of the TKE dissipation rate.

Acknowledgements

The authors wish to thank the anonymous reviewers for their careful and comprehensive evaluation of the paper and their helpful comments, both of which improved the quality of this work.

References

Baker, T.C., Fadamiro, H.Y., Cosse, A.A., 1998. Moth uses fine tuning for odour resolution. Nature 393 (6685), 530.

Cassiani, M., Franzese, P., Giostra, U., 2005a. A PDF micromixing model of dispersion for atmospheric flow. Part I. Development of model, application to homogeneous turbulence and to a neutral boundary layer. Atmos. Environ. 39, 1457–1469.

Cassiani, M., Franzese, P., Giostra, U., 2005b. A PDF micromixing model of dispersion for atmospheric flow. Part II. Application to convective boundary layer. Atmos. Environ. 39, 1471–1479.

Cassiani, M., Radicchi, A., Albertson, J.D., 2007. Modelling of concentration fluctuations in canopy turbulence. Boundary-Layer Meteorol. 122, 655–681.

Cassiani, M., Radicchi, A., Giostra, U., 2005c. Probability density function modelling of concentration in and above a canopy layer. Agric. Forest Meteorol. 133, 153–165.

Chang, J.C., Hanna, S.R., 2004. Air quality performance evaluation. Meteorol. Atmos. Phys. 87, 167–196.

Coppin, P.A., Raupach, M.R., Legg, B.J., 1986. Experiments on scalar dispersion within a model plant canopy. Part 2. An elevated plane source. Boundary-Layer Meteorol. 35, 167–191.

Flesch, T.K., Wilson, J.D., 1992. A two-dimensional trajectory-simulation model for non-Gaussian, inhomogeneous turbulence within plant canopies. Boundary-Layer Meteorol. 61, 349–374.

Fox, R.O., 1996. On velocity-conditioned scalar mixing in homogeneous turbulence. Phys. Fluids 8, 2678–2691.

Franzese, P., 2003. Lagrangian stochastic modelling of a fluctuating plume in the convective boundary layer. Atmos. Environ. 37, 1691–1701.

Gailis, R.M., Hill, A., Yee, E., Hilderman, T., 2007. Extension of a fluctuating plume model of tracer dispersion to a sheared boundary layer and to a large array of obstacles. Boundary-Layer Meteorol. 122, 577–602.

Gifford, F.A., 1959. Statistical properties of a fluctuating plume dispersion model. Adv. Geophys. 6, 117–137.

Gillette, N., Erbilgin, N., Webster, J., Pederson, L., Mori, S., Stein, J., Owen, D., Bischel, K., Wood, D., 2009. Aerially applied verbenone-releasing laminated flakes protect *Pinus contorta* stands from attack by *Dendroctonus ponderosae* in California and Idaho. Forest Ecol. Manage. 257, 1405–1412.

Graves, A.D., Holsten, E.H., Ascerno, M.E., Zogas, K.P., Hard, J.S., Huber, D.P., Blanchette, R.A., Seybold, S.J., 2008. Protection of spruce from colonization by the bark beetle, *Ips perturbatus*, in Alaska. Forest Ecol. Manage. 256, 1825–1839.

Hilderman, T., Chong, R., 2007. A laboratory study of momentum and passive scalar transport and diffusion within and above a model urban canopy – final report. DRDC Suffield CR 2008-025. Technical Report. Defence R&D Canada - Suffield, Ralston, Alberta, 78 pp.

Hsieh, K.J., Lien, F.S., Yee, E., 2007. Numerical modeling of passive scalar dispersion in an urban canopy layer. J. Wind Eng. Ind. Aerodyn. 95, 1611–1636.

Legg, B.J., Raupach, M.R., Coppin, P.A., 1986. Experiments on scalar dispersion within a model plant canopy. Part 3. An elevated line source. Boundary-Layer Meteorol. 35, 277–302.

Luhar, A.K., Hibberd, M.F., Borgas, M.S., 2000. A skewed meandering plume model for concentration statistics in the convective boundary layer. Atmos. Environ. 34, 3599–3616.

Luhar, A.K., Sawford, B.L., 2005. Micromixing modelling of concentration fluctuations in inhomogeneous turbulence in the convective boundary layer. Boundary-Layer Meteorol. 114, 1–30.

Murlis, J., 1997. Odor plumes and the signals they provide. In: Cardé, R.T., Minks, A.K. (Eds.), Pheromone Research: New Directions. Chapman and Hall, New York, pp. 221–231.

Murlis, J., Elkinton, J.S., Cardé, T., 1992. Odor plumes and how insects use them. Annu. Rev. Entomol. 37, 505–532.

Poggi, D., Katul, G.G., Albertson, J., 2006. Scalar dispersion within a model canopy: measurements and three-dimensional Lagrangian models. Adv. Water Resour. 29, 326–335.

Pope, S.B., 1998. The vanishing effect of molecular diffusivity on turbulent dispersion: implications for turbulent mixing and the scalar flux. J. Fluid Mech. 359, 299–312.

Postma, J.V., Wilson, J.D., Yee, E., 2011a. Comparing two implementations of a micromixing model. Part I. Wall shear-layer flow. Boundary-Layer Meteorol. 140, 207–224.

Postma, J.V., Wilson, J.D., Yee, E., 2011b. Comparing two implementations of a micromixing model. Part II. Canopy flow. Boundary-Layer Meteorol. 140, 225–241.

Postma, J.V., Yee, E., Wilson, J.D., 2012. First-order inconsistencies caused by rogue trajectories. Boundary-Layer Meteorol, http://dx.doi.org/10.1007/s10546-012-9732-7.

Raupach, M.R., Coppin, P.A., Legg, B.J., 1986. Experiments on scalar dispersion within a model plant canopy. Part 1. The turbulence structure. Boundary-Layer Meteorol. 35, 21–52.

Rodean, H.C., 1996. Stochastic Lagrangian Models of Turbulent Diffusion. American Meteorological Society, 84 pp.

Savitzky, A., Golay, M.J.E., 1964. Smoothing and differentiation of data by simplified least squares procedures. Anal. Chem. 36, 1627–1639.

Sawford, B.L., 2004a. Conditional scalar mixing statistics in homogeneous isotropic turbulence. New J. Phys. 6, 1–30.

Sawford, B.L., 2004b. Micro-mixing modelling of scalar fluctuations for plumes in homogeneous turbulence. Flow Turbul. Combust. 72, 133–160.

Steinier, J., Termonia, Y., Deltour, J., 1972. Comments on smoothing and differentiation of data by simplified least square procedure. Anal. Chem. 44, 1906–1909.

Thomson, D.J., 1987. Criteria for the selection of stochastic models of particle trajectories in turbulent flows. J. Fluid Mech. 180, 529–556.

Thomson, D.J., 1996. The second-order moment structure of dispersing plumes and puffs. J. Fluid Mech. 320, 305–329.

Vickers, N.J., 2000. Mechanisms of animal navigation in odour plumes. Biol. Bull. 198, 203–212.

Wang, B.-C., Yee, E., Lien, F.-S., 2009. Numerical study of dispersing pollutant clouds in a built-up environment. Int. J. Heat Fluid Flow 30, 3–19.

Yee, E., 2009. Probability law of concentration in plumes dispersing in an urban area. Environ. Fluid Mech. 9, 389–407.

Yee, E., Chan, R., Kosteniuk, P.R., Chandler, G.M., Biltoft, C.A., Bowers, J.F., 1994. Incorporation of internal fluctuations in a meandering plume model of concentration fluctuations. Boundary-Layer Meteorol. 67, 11–39.

Yee, E., Wang, B.-C., Lien, F.-S., 2009. Probabilistic model for concentration fluctuations in compact-source plumes in an urban environment. Boundary-Layer Meteorol. 130, 169–208.

Yee, E., Wilson, D.J., 2000. A comparison of the detailed structure in dispersing tracer plumes measured in grid-generated turbulence with a meandering plume incorporating internal fluctuations. Boundary-Layer Meteorol. 94, 253–296.